RADIOFOREGROUNDS.
D4.1 – Three-dimensional parametric Galactic magnetic field models

Authors: Vincent Pelgrims
Juan Francisco Macías-Pérez
Céline Combet

Date: July 25, 2017

1 Introduction

Our Galaxy is filled by an interstellar magnetic field that has an average strength of a few microgauss (see e.g. Planck Collaboration Int. XIX 2015 for a review). This magnetic field lies in the entire disk of our Galaxy and extends at high Galactic latitudes into the halo. The Galactic magnetic field (GMF) appears to be inhomogeneous and shows rapid spatial variations in magnitude and orientation. Some matter constituents of the Galaxy, such as dust grains or relativistic electrons, are sensitive to the ambient magnetic field. Matter and magnetic field couple in a way that leads to the emission of polarized light. From radio to submillimeter wavelengths, the Galactic polarized diffuse emission is due to synchrotron emission below about 80 GHz and thermal dust emission above. This diffuse emission comes from relativistic electrons that spiral along the lines of the magnetic field for synchrotron and from aspherical dust grains in rotation about the field lines for the thermal dust.

In polarization, the synchrotron and the thermal dust Galactic diffuse emissions dominate the signal in the whole frequency range covered by the Cosmic Microwave Background (CMB) radiation. Consequently, these emissions constitute significant Galactic foregrounds that need to be accurately handled in order to extract cosmological signal. This motivates further the understanding and the physical modelization of the two polarized emissions and thus of the Galactic magnetic field. The large-scale geometrical structure of the GMF is indeed deeply involved in the polarization channels as it can be noticed from a relatively simple modelization of these emission mechanisms. Therefore sky maps of the synchrotron and of the thermal dust polarized emissions may be used to study and constrain GMF models. This is part of the scientific goal of the WP4.2 of the European H2020 RADIOFOREGROUNDS project. Because of its importance for CMB cosmology, the diffuse polarized emissions have been recorded with very high precision and in different frequency bands during the two last decades. The wealth of information present in these full-sky observations are extremely valuable for modeling the various components of the Galaxy. An appropriate combination of existing data sets should provide strong constraints on GMF models and also on the Galactic matter density distribution.

This document is structured as follows. In Section 2, we briefly review the formalism of the modeling of the diffuse Galactic emissions (thermal dust and synchrotron) upon which we base our discussion. In Section 3, we provide a short review of the regular magnetic field models that have already been investigated in the literature and from which a new model shall be build by the end of the project. In Section 4, we provide a brief description of the Python module containing Python functions intended to the implementation of those parametric models of the Galactic magnetic field.

2 Modelization of diffuse Galactic emissions

In this section we review the modelization of the Galactic diffuse polarized emissions induced from dust grains and from relativistic electrons. We start with the thermal dust emission which dominates the polarized signal above 80 GHz and that is the only significant foreground of the CMB at those frequencies (e.g., Planck Collaboration Int. XXX 2014). We then turn to the synchrotron emission that dominates the polarized signal below 80 GHz and that also constitutes one of the significant contributions in intensity maps at low frequency.

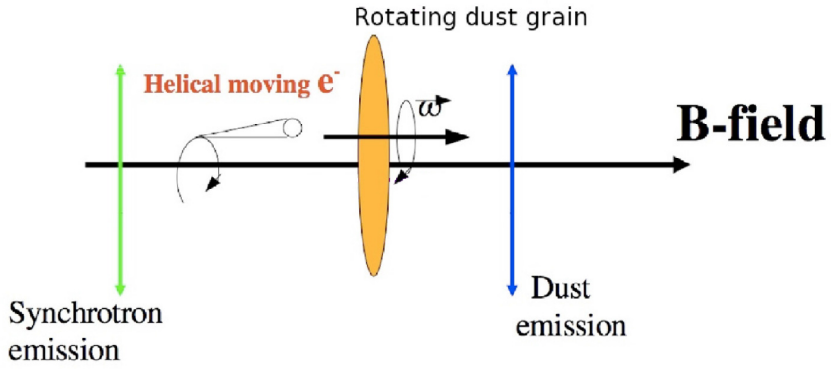

Figure 1: Schematic view of the polarization direction of the Galactic synchrotron and dust thermal emissions as functions of the Galactic magnetic field direction. Figure from Fauvet et al. (2011).

2.1 Thermal dust polarized emission

If the magnetic field is coherent in a given region of the sky, dielectric dust grains tend to align with the field lines in that region (e.g., Fauvet et al., 2011). The thermal diffuse emission from the dust that arises at submillimeter wavelengths is then polarized due to this effective alignment. The polarization of this light is known to be preferentially perpendicular to the projection of the magnetic field lines in which the dust grains are embedded. This is sketched in Figure 1.

Polarized thermal dust has already been used in the past in an attempt to provide constraints on the large-scale magnetic field in the Galaxy. Page et al. (2007) showed that the 94 GHz band of *WMAP*[1] contains some polarization from the thermal dust ; Fauvet et al. (2011) considered the 353 GHz data from the ARCHEOPS[2] balloon as added values to *WMAP* 22 GHz synchrotron to fit a Galactic magnetic field model ; Jaffe et al. 2013 used the full-sky 94 GHz polarization maps from the *WMAP* satellite and showed that this emission is not compatible with the field configuration to fit best the polarized synchrotron of the same experiment ; and recently, Planck Collaboration Int. XLII (2016) used the 353 GHz data from *Planck*[3] to show that thermal dust data are in conflict with prediction from synchrotron data. The two latter works demonstrate the existing limitations of the use of component separation methods in the microwave bands. To date, it is not clear if these discrepancies are due to non-sufficiently elaborate models or if there is more physics behind to be unveiled.

The up-to-date polarization data of the thermal dust are those from the *Planck* satellite at 353 GHz

[1] https://map.gsfc.nasa.gov/
[2] https://fr.wikipedia.org/wiki/Archeops
[3] http://www.esa.int.Planck

(Planck Collaboration Int. XXII, 2015). The Planck Collaboration provided full-sky coverage maps in the three polarization channels, namely the I, Q and U Stokes parameters. These observables are projected quantities resulting from an integration along the line of sight of infinitesimal contributions. To model the diffuse emission from thermal dust, we follow the parameterization of Fauvet et al. (2011) that has also been used in the subsequent analyses (Jaffe et al., 2013; Planck Collaboration Int. XLII, 2016) and, to the best of our understanding, which is also implemented in the HAMMURABI code (Waelkens et al., 2009). Nevertheless, we review their misalignment term. According to a more physically motivated modelization of the emission introduced in Lee & Draine (1985), we attribute a constant value to the misalignment term. However, compared to that dust emission modelization reviewed in (Planck Collaboration Int. XX, 2015, Appendix B), we make the assumption that the intensity of the thermal dust emission is independent of the GMF. Namely, we assumed that the second term in the parenthesis of the top equation in Eqs. 1 is negligible compared to the first term. We plan to test the implication of this assumption on the reconstruction of the GMF model in a simulation-only basis.

Specifically, the modelization that we will use take the form:

$$
\begin{aligned}
I(\mathbf{n}) &= \epsilon_\nu^{\rm dust} \int_0^{+\infty} dr\, n_d(r,\mathbf{n}) \left\{1 + p^{\rm dust}\, f_{\rm ma} \left(\frac{2}{3} - \sin^2\alpha(r,\mathbf{n})\right)\right\} \\
Q(\mathbf{n}) &= \epsilon_\nu^{\rm dust}\, p^{\rm dust}\, f_{\rm ma} \int_0^{+\infty} dr\, n_d(r,\mathbf{n})\, \sin^2\alpha(r,\mathbf{n})\, \cos[2\,\gamma(r,\mathbf{n})] \\
U(\mathbf{n}) &= \epsilon_\nu^{\rm dust}\, p^{\rm dust}\, f_{\rm ma} \int_0^{+\infty} dr\, n_d(r,\mathbf{n})\, \sin^2\alpha(r,\mathbf{n})\, \sin[2\,\gamma(r,\mathbf{n})]
\end{aligned}
\tag{1}
$$

where r is the radial distance from the observer, $\mathbf{n}$ represents sky coordinates and the different terms are

- $\epsilon_\nu^{\rm dust}$ is the dust emissivity at frequency ν which is linked to the dust temperature through the grey-body's law (e.g. Planck Collaboration Int. XX, 2015, Appendix B)
- $p^{\rm dust}$ is the so-called intrinsic degree of linear polarization of the dust that depends on the specifics of the dust grains. It represents the maximum value of the degree of linear polarization of the radiation emitted by an hypothetical ensemble of perfectly aligned dust grains from a small volume
- $f_{\rm ma}$ is the misalignment term that, in general should depend on the dust population
- $n_d(r,\,\mathbf{n})$ is the Galactic dust density
- $\alpha(r,\,\mathbf{n})$ is the inclination angle of the GMF line with the line of sight at $(r,\,\mathbf{n})$
- $\gamma(r,\,\mathbf{n})$ is the so-called local polarization angle.

The latter angle is perpendicular to the position angle that makes the GMF vector in the plane orthogonal to the line of sight with respect to the local meridian. Namely, expressed in terms of the vector component of the ambient magnetic field, this angle reads

$$
\gamma(r,\,\mathbf{n}) = \frac{1}{2}\arctan\left(\frac{-2\,B_\theta(r,\,\mathbf{n})\,B_\phi(r,\,\mathbf{n})}{B_\phi(r,\,\mathbf{n})^2 - B_\theta(r,\,\mathbf{n})^2}\right) \tag{2}
$$

with B_θ and B_ϕ the local transverse components of the magnetic field in the local spherical coordinate basis. The latter expression thus gives, in the HEALPix convention (Górski et al., 2005), the polarization position angle of the polarization vectors stemming from the small space volume. This angle is defined in the range $[0,\,180]$.

According to this implementation of the polarized thermal dust emission (and assuming the usual assumption is valid), the Galactic magnetic field is only relevant for the Q and U Stokes parameters. Note that according to this implementation none of the observable depend on the amplitude of the magnetic field but only on its geometrical structure.

2.2 Synchrotron polarized emission

As for thermal dust, a local coherence in the orientation of the Galactic magnetic field lines across a sufficiently large region of space leads to a net polarized emission from relativistic electrons that spiral around those lines (Rybicki & Lightman, 1979). That is the Galactic diffuse synchrotron. It is known to be preferentially perpendicular to the projection of the magnetic field lines as it is the case for the thermal dust emission as illustrated in Figure 1.

The polarized synchrotron emission has been widely used in the literature to constrain the magnetic field of our Galaxy. Page et al. (2007) used three-years full-sky maps in K-band (about 22 GHz) and fit a parametric model using the polarization position angles of the emission ; Ruiz-Granados et al. (2010) used the five-year *WMAP* polarization data at the same frequency and search for the best fits of several parametric models ; Sun et al. (2008), Sun & Reich (2010), Jansson & Farrar (2012a), Jansson & Farrar (2012b) ,Jaffe et al. (2010) and Jaffe et al. (2013) built more sophisticate GMF models and used the same *WMAP* data to constrain them, complementing or not the synchrotron data with Faraday rotation measure on Galactic or extragalactic sources ; and recently, Planck Collaboration Int. XLII (2016) used the synchrotron data from the *Planck* satellite to upgrade few magnetic field models obtained from *WMAP* data and rotation measure data. The latter study show the limitation of the current model at reproducing the current data sets.

The up-to-date synchrotron data come from different instruments, regarding the specific frequency band. Full-sky data are from the *WMAP* and *Planck* satellite. Currently, QUIJOTE[4] is providing high quality polarization data at low frequencies, but for the North equatorial hemisphere only. The combination of numerous wavelength observations is promising at better constraining the models of the Galactic diffuse synchrotron emission and so of the Galactic magnetic field.

For the synchrotron emission we follow the model emission by Rybicki & Lightman (1979) and we adopt the notation of Fauvet et al. (2011). Let introduce $\mathbf{B}_\perp(r,\mathbf{n})$ the magnetic field vector projected on the plane of the sky, i.e., orthogonal to the line of sight pointing in the direction $\mathbf{n}$. If ϵ_ν is an emissivity term for the synchrotron emission, $n_e(r,\mathbf{n})$ the three-dimensional density of the relativistic (cosmic-ray) electrons that spiral along the magnetic field line and s the spectral index of the energy distribution of the relativistic electrons in the Galaxy, then the Stokes parameters take the following expression:

$$
\begin{aligned}
I(\mathbf{n}) &= \epsilon_\nu^{\rm sync} \int_0^{+\infty} dr\, n_e(r,\mathbf{n})\, \left(\mathbf{B}_\perp(r,\mathbf{n})^2\right)^{(s+1)/4} \\
Q(\mathbf{n}) &= \epsilon_\nu^{\rm sync}\, p_{sync} \int_0^{+\infty} dr\, n_e(r,\mathbf{n})\, \left(\mathbf{B}_\perp(r,\mathbf{n})^2\right)^{(s+1)/4} \cos[2\gamma(r,\mathbf{n})] \\
U(\mathbf{n}) &= \epsilon_\nu^{\rm sync}\, p_{sync} \int_0^{+\infty} dr\, n_e(r,\mathbf{n})\, \left(\mathbf{B}_\perp(r,\mathbf{n})^2\right)^{(s+1)/4} \sin[2\gamma(r,\mathbf{n})]
\end{aligned}
\tag{3}
$$

where $\epsilon_\nu^{\rm sync}$ is the synchrotron emissivity, $n_e(r,\mathbf{n})$ is the local density of relativistic electrons, p_{sync} is the intrinsic synchrotron polarization fraction which is related to the electron energy spectral index as:

$$
p_{sync} = \frac{s+1}{s+7/3}\,. \tag{4}
$$

The angle γ found in the expression of Q and U is the same as in Eq.2. It is computed as being perpendicular to the position angle of the GMF projected on to the plane orthogonal to the line of sight at each position in the space. Notice that $\mathbf{B}_\perp(r,\mathbf{n})^2 = \mathbf{B}(r,\mathbf{n})^2 \sin^2[\alpha(r,\mathbf{n})]$ where the angle $\alpha(r,\mathbf{n})$ is the same as in 1, i.e. is the inclination angle of the GMF vector with respect to the line of sight. As a consequence, if one assumes the relativistic electron spectral index to be 3 then the Stokes Q and U of the synchrotron emission exhibit the same dependence on α and γ as those of the thermal dust emission. The fundamental difference between the two emissions is that the synchrotron emission depends on the (total) amplitude of the magnetic field while dust emission does not. Note that fixing

[4] http://www.iac.es/proyectos.php?op1=7&op2=21&id=27&lang=en

$s = 3$ for the whole sky was assumed in all papers cited above that attempted to model and reproduce the all-sky synchrotron emission. This issue has not been considered yet in the framework of large-scale Galactic magnetic field reconstruction.

3 Parametric Galactic magnetic field models

Several parametric models have been published in the literature to account for the large-scale Galactic magnetic field. Due to geometrical structure similarities that the different models produce, only three of them – thought to summarize somehow the variety of models – have been used to fit the *Planck* polarized foreground data (Planck Collaboration Int. XLII, 2016). As part of the RADIOFOREGROUNDS project deliverable, we aim at providing a compilation of (as much as possible) parametric models to be compared with the several data sets from the different instruments and at different wavelengths. Those parametric models will be implemented in dedicated Python software that will be made publicly available[5] and that already contains few of those implementations. Some of those parametric magnetic fields have been already reviewed by Ruiz-Granados et al. (2010). The other models that we are planning to consider were recently discussed in (Planck Collaboration Int. XLII, 2016). Note that at a first stage we will consider mainly the 'coherent' components of the models discussed in that paper. As mentioned by Ruiz-Granados et al. (2010), it is fair to focus on the large-scale field only as far as we consider large-scales, e.g. above 100 pc. For the random GMF component, we consider only the possibility to generate some isotropic random field thought to reproduce a turbulent magnetic field component (e.g., Jaffe et al., 2010; Fauvet et al., 2011).

A common feature of the parametric modeling of these different 'coherent' or 'large-scale' (or even 'regular') component of the GMF is that the analytical form is expressed in cylindrical coordinates centered on the Galactic center. In the literature, several conventions were adopted to define the reference frame and to describe the geometrical structure of the Galactic magnetic field. We adopt the following one. We define the cylindrical coordinates $(\rho,\, \phi,\, z)$ of the Galactocentric reference frame as

$$\begin{aligned} \rho =& (x^2 + y^2)^{1/2} \\ \phi =& \arctan(y/x) \\ z =& z \end{aligned} \tag{5}$$

where the right-hand side coordinates $(x,\, y,\, z)$ are the Galactocentric Cartesian coordinates. The relation to the spherical coordinates of the observer, i.e. in the heliocentric reference frame, reads

$$\begin{aligned} x =& -R_\odot + r\, \cos(l)\cos(b) \\ y =& r\, \sin(l)\cos(b) \\ z =& r\, \sin b \end{aligned} \tag{6}$$

where $(l,\, b)$ are the Galactic longitude and latitude of the observed sky position, r the radial distance to the observer and $R_\odot$ is the distance between the Sun and the Galactic center that we set to 8.0 kpc. Following this scheme illustrated in Figure 2, the Sun is located at $(-R_\odot,\, 0,\, 0)$ in the Galactocentric Cartesian coordinate system, the y-axis is positive towards $l = 90°$ and the polar angle ϕ increases counter-clockwise in the $(x,\, y)$ plane. We have $\mathbf{e}_z = \mathbf{e}_\rho \times \mathbf{e}_\phi$ where $\times$ is the vectorial cross product and where $(\mathbf{e}_\rho,\, \mathbf{e}_\phi,\, \mathbf{e}_z)$ is the orthonormal basis of the cylindrical coordinates system centered on the Galactic center.

Using this basis, the general form of the Galactic magnetic field model is

$$\mathbf{B} = B_\rho \mathbf{e}_\rho + B_\phi \mathbf{e}_\phi + B_z \mathbf{e}_z \tag{7}$$

where, in general, the cylindrical components may be functions of the coordinates. The parametric models that we investigate differ on that functional forms of the coordinates. Below we will give the analytical expression of the following models:

[5] http://www.radioforegrounds.eu/

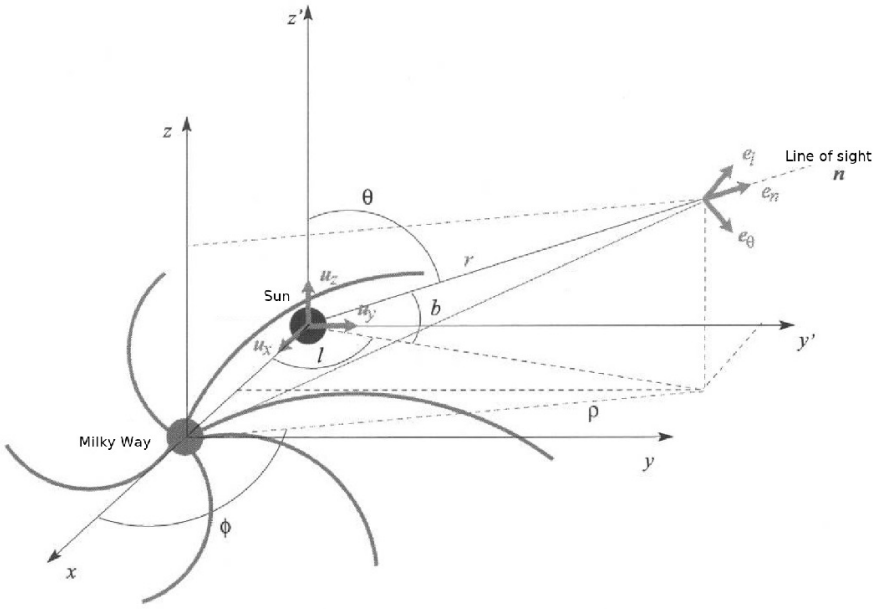

Figure 2: Convention of the different coordinate system used in this work. Figure adapted from Fauvet 2010.

1. AxiSymmetric Spiral
2. Logarithmic Spiral Arm
3. BiSymmetric Spiral
4. Concentric Circular Ring
5. Bi-Toroidal / Halo model
6. Jansson & Farrar model
7. Jaffe et al. model

The two latter models are composite models drawn from the different geometries covered by the five first models. They are thus elaborated models with geometries that vary according to the Galactocentric coordinates. Due to their elaborated nature, a large number of parameters are necessary to describe them.

For all the models, we plane to use Markov Chain Monte Carlo (MCMC) approach to find out the best-fit parameters and their likelihood using polarized diffuse emissions. The optimized codes that are necessary to run MCMC are not part of the sub-routines referred here but will be released separately.

3.1 Axi-Symmetric Spiral (ASS) model

The axisymmetric model (see e.g., Vallee, 1991; Poezd et al., 1993) is one of the simplest descriptions of the Galactic magnetic field. It is compatible with a non-primordial origin of the galactic magnetism,

based on the dynamo theory. The field lines follow logarithmic spirals with constant pitch angle. The cylindrical components for this model of magnetic field are:

$$\begin{aligned} B_\rho &= B_0 \sin(p) cos(\chi(z)) \\ B_\phi &= B_0 \cos(p) cos(\chi(z)) \\ B_z &= B_0 \sin(\chi(z)) \end{aligned} \tag{8}$$

where p is the pitch angle, which is considered to be constant in this model, B_0 is the field strength that might, in general, depend on the distance to the Galactic center and $\chi(z)$ is some 'tilt angle' that allows the field lines to exit the planes parallel to the Galactic plane. The pitch angle is defined as the angle between the azimuthal direction $\mathbf{e}_\phi$ and the magnetic field[6]. $p = 0°$ corresponds to circle, $p = 90°$ produces (cylindrical) radial lines.

The 'tilt angle' is usually taken as

$$\chi(z) = \chi_0 \tanh\left(\frac{z}{z_0}\right) . \tag{9}$$

The parameters χ_0 and z_0 are not independent and the usual choice is to fix the height scale as $z_0 = 1$ kpc.

Different modelization of the field strength 'radial' dependence exist. First, B_0 is sometimes set to a constant value throughout space (e.g., Page et al., 2007). In this case the Galactic magnetic field has the same amplitude everywhere in space, which is not well physically motivated. Based on Faraday rotation measures, Han et al. 2006 have proposed a (spherical) radial dependence of the form

$$B_0(r_{\rm G}) = B_\odot \exp\left(\frac{-(r_{\rm G} - R_\odot)}{R_{\rm B}}\right) \tag{10}$$

where $r_{\rm G}$ is the spherical radial distance to the center of the Galaxy ($r_{\rm G} = \sqrt{\rho^2 + z^2}$) and $B_\odot$ is the strength of the magnetic field at the Sun radius, measured to be about 3 μG. This implementation was used in Fauvet et al. (2011). Another modelization of the field strength was suggested in Ruiz-Granados et al. (2010) to extend the model by Poezd et al. (1993). This functional form involves the cylindrical-radial distance only:

$$B_0(\rho) = \frac{B_1}{1 + \rho/\rho_1} . \tag{11}$$

In those two parameterizations, the parameters are not independent. We can restrict the equation with the known solution, by injecting the local value of the strength field. Indeed, we know that the magnetic field strength in the Sun neighborhood is measured to be of about 3 μG. The number of free parameters in these models of the field strength are therefore readily reduced to one.

Under the class of axisymmetric spiral models, we already have three different models to test: ASS, with $B_0 = constant$, and ASSρ and ASSr, with the cylindrical- and spherical- radial dependence of the field strength. They all have three free parameters that can be fitted to the data. Notice that the comparison between ASSρ and ASSr had never been explored. Also, the choice of the values of the other parameters (such as z_0) and their impact on the best fit model had never been tested rigorously. We plan to proceed to such investigations.

3.2 Logarithmic Spiral Arm (LSA) model

This model was introduced in Page et al. (2007) to describe the 3-year WMAP data at 22 GHz for the synchrotron emission and at 94 GHz for the thermal dust emission. Basically, it implements an extension

[6] Notice that there is no convention for measuring the pitch angle. An opposite value possibly indicates the use of another convention.

of the ASS class of models where the pitch angle defining the spiral structure depends on the cylindrical radius. Consequently, and despite the name of the model, the spirals are *not* logarithmic. In addition, there is no arm structure in the field amplitude.

The component parametric forms read

$$\begin{aligned} B_\rho &= B_0 \sin(\psi(\rho)) \cos(\chi(z)) \\ B_\phi &= B_0 \cos(\psi(\rho)) \cos(\chi(z)) \\ B_z &= B_0 \sin(\chi(z)) \end{aligned} \tag{12}$$

where the function

$$\psi(\rho) = \psi_0 + \psi_1 \ln\left(\frac{\rho}{8.0\,\mathrm{kpc}}\right) \tag{13}$$

forces the magnetic field lines to follow a spiral pattern with varying pitch angle. The 'tilt angle' $\chi(z)$ is taken as in Eq. 9 with $z_0 = 1$ kpc. While Page et al. (2007) considered B_0 to be constant through space, we shall allow for the same radial dependence as for the ASS class of models. This would particularly be relevant for the case of synchrotron emission as the norm, though projected on the polarization plane, appears in the intensity (Rybicki & Lightman, 1979) and thus in Q and U Stokes as modeled in Fauvet et al. (2011).

Having fixed B_0 (to a constant or with the parameterization from Eq. 10 or Eq. 11), the LSA models have three free parameters to be fixed by the data. The best-fit values obtained by Page et al. (2007) are $\psi_0 = 27°$, $\psi_1 = 0.9°$ and $\chi_0 = 25°$. We have run Markov Chain Monte Carlo on those models and we have identified degeneracies in these parameters. The impact of these degeneracies on the reconstructed Galactic magnetic field model still need to be properly assessed.

3.3 Bisymmetric (BSS) model

The class of bisymmetric spiral models produces Galactic magnetic fields compatible with a primordial origin. This model includes magnetic field reversion as suggested from pulsar rotation measurements (e.g., Han & Qiao, 1994; Han et al., 2006). The spirals featured in this field model have constant pitch angle. The cylindrical components of this field model read

$$\begin{aligned} B_\rho &= B_0 \cos\left(\phi \pm \beta \ln\left(\frac{\rho}{R_\odot}\right)\right) \sin(p) \cos(\chi(z)) \\ B_\phi &= B_0 \cos\left(\phi \pm \beta \ln\left(\frac{\rho}{R_\odot}\right)\right) \cos(p) \cos(\chi(z)) \\ B_z &= B_0 \sin(\chi(z)) \end{aligned} \tag{14}$$

where $\beta = 1/\tan(p)$, with p the pitch angle, $R_\odot$ the distance between the Sun and the Galactic center, $\chi(z)$ the 'tilt angle' defined as in Eq. 9 and B_0 the field strength that can be either a constant, or some function of the coordinates as described in Eqs. 10 and 11. Notice however that the amplitude of the field is already shaped in spirals by the term $\cos\left(\phi \pm \beta \ln\left(\frac{\rho}{R_\odot}\right)\right)$ which also produces field inversion. The $\pm$ in the parentheses was introduced by Ruiz-Granados et al. (2010) to account for the different conventions met in the literature. Given our working scheme presented through Eqs. 5 and 6, we should adopt the '$-$' sign so that the spiral pattern of the GMF amplitude and of the GMF lines coincide, which is reasonable to postulate.

As the two classes of parametric magnetic field models discussed above, the bisymmetric models have three free parameters that can be fitted by the observations. This model was also referred to as the 'Modified Logarithmic Spiral' model in Fauvet et al. (2011). The minus sign in the expression of B_ϕ of Fauvet et al. (2011) is likely due to the opposite convention for increasing azimuth angle.

3.4 Concentric Circular Ring (CCR) model

The class of Concentric Circular Ring (CCR) models was introduced in 1989 to fit the rotation measurements of pulsars and to account for the reversals of the magnetic field. This model was revisited latter and reviewed in Ruiz-Granados et al. (2010). The cylindrical components of this model have the following expression:

$$\begin{aligned} B_\rho &= 0 \\ B_\phi &= \frac{B_0}{\sin(\pi D_r/\omega)} \sin\left(\frac{\pi(\rho - R_\odot + D_r)}{\omega}\right) \cos(\chi(z)) \\ B_z &= B_0 \sin(\chi(z)) \end{aligned} \tag{15}$$

where ω is the (radial) distance between reversals, D_r is the distance to the first reversal and B_0 and $\chi(z)$ are the field strength and the 'tilt angle' defined as before. For this class with concentric magnetic field lines, no radial dependence of the field strength has ever been considered.

The CCR models have four free parameters that can be fitted to observations. Compared to more recent parametric GMF models, the class of CCR seems a bit deprecated as more general geometrical structures can be found in other implementation with magnetic field reversals such as in BSS models.

3.5 Bi-Toroidal model (Halo model)

According to pulsar rotation measurements, some authors have claimed for the need of a magnetic field component of the halo showing opposite directions in both hemispheres (see Sun et al., 2008, and references therein). Different implementations of a parametric GMF model that can account for such behavior have been proposed. We follow the one implemented in (Sun et al., 2008; Sun & Reich, 2010) and that has been fitted to the data in Planck Collaboration Int. XLII (2016).

The purely bitoroidal (BT) model has cylindrical components

$$\begin{aligned} B_\rho &= 0 \\ B_\phi &= \mathrm{sign(z)}\, \mathrm{B_0} \frac{1}{1 + \left(\frac{|\mathrm{z}| - \mathrm{z_0}}{\mathrm{z_1}}\right)^2} \frac{\rho}{\rho_0} \exp\left(-\frac{\rho - \rho_0}{\rho_0}\right) \\ B_z &= 0 \end{aligned} \tag{16}$$

where the function $\mathrm{sign(z)}$ takes the sign of z and where z_0, z_1 and ρ_0 are parameters that depend on the thermal electron density that follows an exponential disk model (Sun & Reich, 2010). B_0 is the field strength defined as usual.

It is important to keep in mind that this model should add up to an ASS model or to a BSS model as prescribed by the authors. Indeed, in Sun & Reich (2010), the author fitted pulsar rotation measure data and synchrotron data from WMAP with (*i*) an ASS+RING model, (*ii*) an ASS+ARM model and (*iii*) a BSS; all added to the BT model in order to account for the rotation measurement data at high Galactic latitudes. They found that the ASS+RING+BT and ASS+ARM+BT fit well the data while BSS+BT does not. Notice that the RING magnetic field component is simply a non vanishing azimuthal component with a constant amplitude within the 'ring' region defined by its inner and outer radii. For the RING component, $B_\rho = B_z = 0$.

The height dependence of B_ϕ might look not physical as implemented in Sun & Reich (2010) due to very steep variations. To that concern, Ruiz-Granados et al. (2010) proposed a smoother dependence on z. However, the model as implemented in their Eq. (9b) does not produce toroidal shape in the magnetic field. In our model implementation we should allow for the replacement of the steep z-dependence of the original analytical form by the smoother one from Ruiz-Granados et al. (2010). In that implementation we will keep the radial dependence from the original model in order to have toroidal shape. In this

alternative implementation, the azimuthal component of the magnetic field should then read:

$$B_\phi = B_0 \arctan\left(\frac{z}{\sigma_1}\right) \exp\left(\frac{-z^2}{2\sigma_2^2}\right) \frac{\rho}{\rho_0} \exp\left(-\frac{\rho-\rho_0}{\rho_0}\right) . \tag{17}$$

Notice that the addition of the BT model to an ASS or a BSS or a RING model increases considerably the number of parameters to be fitted to the data.

3.6 Jansson & Farrar model

This model proposed in (Jansson & Farrar, 2012a,b) is a composite of distinct components: (*i*) a disk field with circular and spiral geometry depending on the radius to the Galactic center, (*ii*) a halo field with a (bi-)toroidal pattern and (*iii*) an 'out-of-plane' component, called the 'X-field', that is axisymmetric and poloidal, i.e., that has no azimuthal dependence.

In their modelization, Jansson & Farrar (2012a) considered physically motivated conditions that the model has to verify such as divergence-free field. This elaborated model has many free parameters that can be fitted by the data. Jansson & Farrar (2012a,b) used MCMC approach to fit pixelized sky-map of Faraday rotation measurement (from extragalactic sources) and Galactic synchrotron emission from WMAP at 22 GHz. They did not include pulsar rotation measurement.

The model is constructed as follows. The large-scale regular field is a weighted sum of the disk and the halo components of the GMF, $\mathbf{B}^{\rm disk}$ and $\mathbf{B}^{\rm halo}$ respectively. The weight is a function of the Galactocentric coordinates which also gives the height dependence of the disk field components which is assumed symmetrical about the $(x,\, y)$-plane of the Galaxy. The regular field can thus be expressed as

$$\mathbf{B} = (1 - L(z,\, h_{\rm disk},\, \omega_{\rm disk}))\, \mathbf{B}^{\rm disk} + L(z,\, h_{\rm disk},\, \omega_{\rm disk}) \mathbf{B}^{\rm halo} \tag{18}$$

where the weighting function $L(z,\, h,\, \omega)$ has the form

$$L(z,\, h,\, \omega) = \frac{1}{1 + \exp(-2\frac{|z|-h}{\omega})} \tag{19}$$

where h controls the height from which the halo field starts to dominate the disk field and ω sets the width and the steepness of the transition. L approaches a step function for small ω values.

The disk component of the GMF consists of (*i*) a 'molecular ring' between 3 and 5 kpc with circular magnetic field with constant strength and (*ii*) a spiral pattern between 5 and 20 kpc with logarithmic spiral field lines that goes inwards or outwards of the Galactic center. There is also an overall modulation of the field magnitude in $1/\rho$. The field strength and the field direction are defined in eight well separated regions of the space. These regions are defined by eight dividing lines that are logarithmic spirals following the parametric form: $\rho(\phi) = \rho_{-x} \exp(\phi \tan(p))$ where $p = 11.5°$ is the pitch angle[7] shared by all the spirals and ρ_{-x} are the radii at which the spirals cross the negative x-axis. These values are tabulated as $\rho_{-x} = 5.1,\, 6.3,\, 7.1,\, 8.3,\, 9.8,\, 11.4,\, 12.7,\, 15.5$ kpc and are not considered as free parameters of the model. The field strength in each region is a free parameter and is determined by its value at $\rho = 5$ kpc, as shown in Eq. 21. There are seven free parameters describing the field strength in the Galactic plane because, for magnetic flux conservation, it is required that $\sum_{i=1}^{8} f_i b_i = 0$ where b_i is the field strength in the ith-region and f_i is the relative cross-sectional area of the spiral, measured at a given radius. The f_i's can be derived from the tabulated ρ_{-x}'s and have values $0.130,\, 0.165,\, 0.094,\, 0.122,\, 0.13,\, 0.118,\, 0.084,\, 0.156$.

[7] Jansson & Farrar (2012a) un-correctly stated that this is the complement angle which does not correspond to their figure and their implementation of the field direction $\hat{\mathbf{B}}$.

The cylindrical components of the disk component of the GMF can be parameterized as follows:

$$
\begin{aligned}
B_\rho^{\rm disk} &= \begin{cases} 0 & \text{if } \rho < 3\text{kpc} \\ 0 & \text{if } 3 \le \rho < 5\text{kpc} \\ B^{\rm disk}(\rho,\,\phi) L(z, h_{\rm disk}, -\omega_{\rm disk}) \sin(p) & \text{if } \rho \ge 5\text{kpc} \end{cases} \\
B_\phi^{\rm disk} &= \begin{cases} 0 & \text{if } \rho < 3\text{kpc} \\ B^{\rm ring} L(z, h_{\rm disk}, -\omega_{\rm disk}) & \text{if } 3 \le \rho < 5\text{kpc} \\ B^{\rm disk}(\rho,\,\phi) L(z, h_{\rm disk}, -\omega_{\rm disk}) \cos(p) & \text{if } \rho \ge 5\text{kpc} \end{cases} \\
B_z^{\rm disk} &= 0\,. \qquad (20)
\end{aligned}
$$

where we use the relation $L(z,\,h,\,-\omega) = (1 - L(z,\,h,\,\omega))$. For $\rho \ge 5$ kpc, the amplitudes of the radial and azimuthal components of the field $B^{\rm disk}(\rho,\,\phi)$ depend on the specific regions of the polar coordinates that are divided in spirals as explained above. We implement this dependence as:

$$
B^{\rm disk}(\rho,\,\phi) = \sum_{i=1}^{8} B_i^{\rm disk}(\rho,\,\phi) \qquad (21)
$$

with

$$
B_i^{\rm disk}(\rho,\,\phi) = \begin{cases} b_i/(\rho - 5\text{kpc}) & \text{if } \phi_i(\rho) \le \phi < \phi_{i+1}(\rho) \\ 0 & \text{otherwize} \end{cases} \qquad (22)
$$

where $\phi_i(\rho) = \ln(\rho/\rho^i_{-x})/\tan(p)$ parameterizes the logarithmic spiral, i runs from 1 to 8 and ϕ_9 corresponds to ϕ_1. The b_i's give the magnetic field strengths at $\rho = 5$ kpc, modulo the height dependence encoded in $L(z,\,h,\,\omega)$, and are free parameters to be fitted.

Added to the disk component, the halo component which is a purely bi-toroidal, i.e. azimuthal, component which takes the form

$$
\begin{aligned}
B_\rho^{\rm tor} &= 0 \\
B_\phi^{\rm tor} &= \exp(-|z|/z_0)\, L(z, h_{\rm disk}, \omega_{\rm disk}) \\
&\quad \times \begin{cases} B_{\rm n}(1 - L(\rho, \rho_{\rm n}, \omega_{\rm h})) & \text{if z} > 0 \\ B_{\rm s}(1 - L(\rho, \rho_{\rm s}, \omega_{\rm h})) & \text{if z} < 0 \end{cases} \\
B_z^{\rm tor} &= 0\,. \qquad (23)
\end{aligned}
$$

This halo component of the GMF has an exponential scale height, and separate field amplitudes in the north and south, $B_{\rm n}$ and $B_{\rm s}$, respectively. The northern (southern) radial extent of the halo field is set by $\rho_{\rm n}$ ($\rho_{\rm s}$). The parameter $\omega_{\rm h}$ controls the width of the region where the halo field is cut off. Jansson & Farrar (2012a) stated that they considered several forms for the halo field, including axisymmetric and bisymmetric spirals, and settled on the purely toroidal model when it was clear that it led to a superior fit to data. We shall adopt the latter.

As such, the parametric model produces magnetic field lines that are parallel to the Galactic plane. In order to provide a more realistic model, Jansson & Farrar (2012a) introduced a z-component, their so-called 'out-of-plane' component, that is intended to reproduce the X-shape that is observed in radio observations of the magnetic field of extragalactic edge-on galaxies. The z-component is axisymmetric and poloidal. It has no azimuthal component and it is required that the field is divergenceless.

The field strength and the field line at any position $(\rho,\,z)$, are specified by the radius $\rho_{\rm p}$ at which the field line crosses the Galactic plane. The shape and the strength of the field then depend on the value of $\rho_{\rm p}$ compared to a critical Galactocentric radius $(\rho_{\rm X}^{\rm c})$ that is one of the free-parameter of the model. The implementation of Jansson & Farrar 2012a can be parameterized as follows. We have: $\mathbf{B}_{\rm X} = B_\rho^{\rm X}\mathbf{e}_\rho + B_z^{\rm X}\mathbf{e}_z$ where

$$
\begin{aligned}
B_\rho^{\rm X} &= B_{\rm X}(\rho,\,z)\cos\left(\Theta(\rho,\,z)\right) \\
B_z^{\rm X} &= B_{\rm X}(\rho,\,z)\sin\left(\Theta(\rho,\,z)\right) \qquad (24)
\end{aligned}
$$

with the parametric forms of $B_{\rm X}(\rho,\, z)$ and $\Theta(\rho,\, z)$ that read

$$\rho_{\rm p} \leq \rho_{\rm X}^{\rm c} \Rightarrow \begin{cases} \rho_{\rm p} = \frac{\rho\rho_{\rm X}}{\rho_{\rm X}+|z|/\tan(\Theta_{\rm X}^0)} \\ \Theta_{\rm X} = \arctan\left(|z|/(\rho-\rho_{\rm p})\right) \\ B_{\rm X} = B_{\rm X}^0 \exp\left(\frac{-\rho_{\rm p}}{\rho_{\rm X}}\right)\left(\frac{\rho_{\rm p}}{\rho}\right)^2 \end{cases} \tag{25}$$

$$\rho_{\rm p} > \rho_{\rm X}^{\rm c} \Rightarrow \begin{cases} \rho_{\rm p} = \rho - |z|/\tan(\Theta_{\rm X}^0) \\ \Theta_{\rm X} = \Theta_{\rm X}^0 \\ B_{\rm X} = B_{\rm X}^0 \exp\left(\frac{-\rho_{\rm p}}{\rho_{\rm X}}\right)\left(\frac{\rho_{\rm p}}{\rho}\right) \end{cases} \tag{26}$$

where $\rho_{\rm X}$, $\rho_{\rm X}^{\rm c}$, $B_{\rm X}^0$ and $\Theta_{\rm X}^0$ are free parameters describing the X-shape and that can be fitted to the data. Outside the critical Galactocentric radius $(\rho_{\rm X}^{\rm c})$ the field lines are taken to have a constant elevation $\Theta_{\rm X}^0$ with respect to the Galactic plane. Inside that critical radius the field lines become vertical as the corresponding $\rho_{\rm p}$ approaches zero.

In total, and despite the parameters that are fixed, the GMF of Jansson & Farrar has 20 free parameters to be fitted to the data. Moreover, to the (purely) analytic form of the field presented above, the authors added to their model an anisotropic random field, which they called 'striated random field'. They found that this field is likely aligned with the (regular) large-scale field and that it has the same relative magnitude everywhere in the Galaxy. They also found that when the striated field is aligned with the regular field, there is a degeneracy between the striated field amplitude and the relativistic electron density. The latter is still unfortunately poorly constrained. Notice that this degeneracy should also involve the other GMF components as it can be guessed from the modelization of the emission given in Eqs. 3. The need and the relevance for synchrotron emission of such an additional field component shall be investigated in close collaboration with the WP 4.1 of the RADIOFOREGROUNDS project.

3.7 Jaffe et al. model

The Galactic model proposed in Jaffe et al. (2013) and based on an earlier version Jaffe et al. (2010) was built to fit data in the Galactic plane only. It was then slightly modified in Planck Collaboration Int. XLII (2016) in an attempt to fit the synchrotron and dust full-sky data. This is the version of the Jaffe model that we shall consider.

As for the Jansson & Farrar model, the total GMF is thought to be the addition of a large-scale regular field and of a random field which, in turn, is made of an isotropic and a striated components. In Jaffe et al. (2010) and subsequent papers, these field components are named 'coherent', 'isotropic random' and 'ordered random', respectively.

As for the Jansson & Farrar model, we only describe the parametric regular field below. The need for the addition of random fields and the way we shall implement them are postponed.

The large-scale regular magnetic field of Jaffe et al. (2010) resemble the disk component of the Jansson & Farrar model. However, the spatial variation of the amplitude and of the direction of the GMF are modeled in a more physical way. Indeed, Jaffe et al. (2013) incorporated continuous transition between arm and inter-arm regions rather than jumping discontinuously from one region to the other, as it is the case in Jansson & Farrar and in the early version of this model (Jaffe et al., 2010). The regular GMF lines are assumed parallel to the Galactic arm where the enhancement of the field strength follows a logarithmic spiral pattern. The last modification of this model, given in Planck Collaboration Int. XLII (2016), follows a double dependence of the vertical profile.

The regular GMF takes the form $\mathbf{B} = \mathbf{B}_{\rm ASS} + \mathbf{B}_{\rm SA}$ with $\mathbf{B}_{\rm ASS}$ an axisymmetric part that models a 'molecular ring' in the inner Galaxy and $\mathbf{B}_{\rm SA}$ the logarithmic spiral arm pattern being the sum of four arms: $\mathbf{B}_{\rm SA} = \sum_{i=1}^{4} \mathbf{B}_{\rm arm,\,i}$ all having the same pitch angle $p = 11.5°$.

The cylindrical components of the GMF components can be parameterized as follows:

$$\begin{aligned} B_\rho &= \begin{cases} 0 & \text{if } \rho < \rho_{\rm ring} \\ B(\rho) \sum_{i=1}^{4} \left(A_i \rho_{\rm c}(d_i)\right) \sin(p) & \text{if } \rho \geq \rho_{\rm ring} \end{cases} \\ B_\phi &= \begin{cases} B(\rho) B_{\rm coh}(z) & \text{if } \rho < \rho_{\rm ring} \\ B(\rho) \sum_{i=1}^{4} \left(A_i \rho_{\rm c}(d_i)\right) \cos(p) & \text{if } \rho \geq \rho_{\rm ring} \end{cases} \\ B_z &= 0 \,. \end{aligned} \tag{27}$$

where

$$B(\rho) = B_0 \exp(-\rho^2/\rho^2_{\rm scale}) \tag{28}$$

$$B_{\rm coh}(z) = B_0^{\rm disk} / \left[\cosh(z/h_{\rm disk})\right]^2 + B_0^{\rm halo} / \left[\cosh(z/h_{\rm halo})\right]^2 \tag{29}$$

$$\rho_{\rm c}(d_i(\rho,\phi), z) = c(\rho) \exp\left[-\left(d_i/d_0(\rho)\right)^2\right] / \left[\cosh(z/h_{\rm c})\right]^2 \tag{30}$$

with d_i the radial distance (along $\mathbf{e}_\rho$) to the ith-arm which are parameterized as

$$\rho_i(\phi) = R_{\rm s} \exp\left[(\phi - \phi_0, i) \tan(p)\right] \tag{31}$$

and

$$\phi_0, i = 10^\circ + 90^\circ i \tag{32}$$

$$c(\rho) = \begin{cases} C_0 & \text{if } \rho \leq \rho_{\rm cc} \\ C_0 (\rho/\rho_{\rm cc})^{-3} & \text{if } \rho > \rho_{\rm cc} \end{cases} \tag{33}$$

$$d_0(\rho) = d_0/(c(\rho)B(\rho)) \,. \tag{34}$$

With no a priori choices, the model has 17 free parameters to be fitted to the data. While it is not specified in Jaffe et al. (2013) and Planck Collaboration Int. XLII (2016), we could choose to fix some of the parameter values as done to fit the Jansson & Farrar model. This shall be investigated. It is quite important to note that this Galactic magnetic field has no out-of-plane component which might significantly impact the high-latitude prediction of the Q and U Stokes parameters of the diffuse emissions and also the synchrotron intensity.

In their model, Jaffe et al. (2013) correlated the amplitude of the matter density distribution with the amplitude of the GMF. This might be an important issue that we shall investigate to fit the thermal dust emission map and the synchrotron emission map. Indeed, the dust density in the Galactic plane also follows a logarithmic spiral arms pattern somehow inspired from the thermal electron density model called 'NE2001' which is due to Cordes & Lazio (2002). Notice that they also correlated the amplitude of the random magnetic field, both the isotropic and the striated components, to the amplitude of the regular component of the GMF.

4 BFIELD Python module

We have developed Python codes that can be used to specify a GMF model. Some of the parametric models described above are already implemented and incorporated to a Python module called `BFIELD`. The other parametric GMF models should be available soon. The `BFIELD` module will be part of a larger code architecture that is intended to produce simulated maps of the foreground diffuse emissions from Galactic relativistic electrons and dust in both intensity and polarization. The whole package is (currently) named `gPemPy` (for Galactic Polarized EMission in PYthon). It will allow for separate modelization of three-dimensional density distribution of matter (dust and/or relativistic electrons) and three-dimensional GMF on the space defining the Galaxy. An additional module will be in charge of producing the corresponding diffuse emission models and to proceed to the integration of the emissions along all the line of sights such as presented, for example, in Eqs. 1 and 3.

The `BFIELD` Python module could be made self-consistent such that it could be used independently from the others. However, for convenience, we deliver it along with another module named `GalaxyBasics` to which it depends through simple functions.

The code can already be found at http://www.radioforegrounds.eu/ and will be made public by the end of the RADIOFOREGROUNDS project along with all the other Python modules of `gPemPy`.

Below, we provide a list the Python functions already implemented in the `BFIELD` module, summarize briefly their effect and provide an idea on how to call the function and the parameters that the user can easily control. We strongly invite the reader to call the `help()` Python function on these functions for a detailed description of what is implemented and what are the various parameters and variables of the functions.

In the `BFIELD` module, there are three different types of functions. First the functions that actually compute the Galactic magnetic field according to their respective parametric modelization; second, some convenience functions that compute relevant quantities for the evaluation of the diffuse emissions and, for example, to convert the three-dimensional vector fields from the Galactocentric reference frame to the heliocentric reference frame; and finally two functions for the visualization of the Galactic magnetic field in cross-cuts of the Galactic space.

4.1 Galactic magnetic field models

- **name:** ASS

  effect: Produces ASS Galactic magnetic field model

  call:
  ```
  ASS(Galactic_coordinates,
      **kwargs{{model_parameter_name:model_parameter_value},
                  coord_format,B_amp_type})
  ```

- **name:** BSS

  effect: Produces BSS Galactic magnetic field model

  call:
  ```
  BSS(Galactic_coordinates,
      **kwargs{{model_parameter_name:model_parameter_value},
                  coord_format,B_amp_type})
  ```

- **name:** LSA

  effect: Produces LSA Galactic magnetic field model

  call:
  ```
  LSA(Galactic_coordinates,
      **kwargs{{model_parameter_name:model_parameter_value},
                  coord_format,B_amp_type})
  ```

- **name:** CCR

  effect: Produces CCR Galactic magnetic field model

  call:
  ```
  CCR(Galactic_coordinates,
      **kwargs{{model_parameter_name:model_parameter_value},
                  coord_format,B_amp_type})
  ```

- **name:** BT

  effect: Produces BiToroidal Galactic magnetic field model

  call:
  ```
  BT(Galactic_coordinates,
     **kwargs{{model_parameter_name:model_parameter_value},
                 coord_format,B_amp_type})
  ```

- **name:** __B_of_r

  effect: Modulates the field amplitude according to radial function, either cylindrical or spherical radial function.

  call:
  ```
  __B_of_r(rho,z,
           **kwargs{{B_0,B_amp_type,B_amp_param,rho_0 }})
  ```

- **name:** ARM4

  effect: Produces a four spiral arm model Galactic magnetic field model

  call:
  ```
  ARM4(Galactic_coordinates,
       **kwargs{{model_parameter_name:model_parameter_value},
                 coord_format,B_of_rho_type,B_of_z_type,B_s_type})
  ```

- **name:** RING

  effect: Produces a RING Galactic magnetic field model

  call:
  ```
  RING(Galactic_coordinates,
       **kwargs{{model_parameter_name:model_parameter_value},
                 coord_format,B_amp_type})
  ```

- **name:** WMAP

  effect: Produces the WMAP Galactic magnetic field model, i.e, of Page et al. 2007

  call:
  ```
  WMAP(Galactic_coordinates,
       **kwargs{{model_parameter_name:model_parameter_value},
                 input_coord_format,withBregular})
  ```

- **name:** MLS

  effect: Produces Modified Logarithmic Spiral Arms model of Fauvet et al. 2010

  call:
  ```
  MLS(Galactic_coordinates,
      **kwargs{{model_parameter_name:model_parameter_value},
                input_coord_format,withBregular})
  ```

- **name:** JAFFE

  effect: Produces the Jaffe et al. Galactic magnetic field model

  call:
  ```
  JAFFE(Galactic_coordinates,
        **kwargs{{model_parameter_name:model_parameter_value},
                  input_coord_format,withBregular})
  ```

- **name:** COMPO

  effect: Allow the addition and the combination of different models such as ARM+RING

  call:
  ```
  COMPO(Galactic_coordinates,
        **kwargs{list_of_Galactic_model:
                  {{model_parameter_name:model_parameter_value}},
                  input_coord_format,withBregular})
  ```

- **name:** B_Regular

  effect: Produces the B field vectors to have spherically exponentially decreasing norm with respect to the Galactic center as proposed by Han et al. 2006

  call:
  ```
  B_Regular(radial_coordinates,amplitude_atSun,
            Sun2GC_distance,radial_scale_parameter)
  ```

- **name:** BFielder

  effect: Populates the Galactic space with magnetic field model given by its name and parameters

  call:
  ```
  BFielder(cartesian_Galactic_coordinates,
           bfield_setup{'model_name':
                        {'name_param_model':
                          value_param_model}})
  ```

- **name:** getBFieldDefault

  effect: Prints (and optionally return) the default settings of the magnetic field model. Shows a complete example of B field initialization and returns it, if nicely asked

  call:
  ```
  getBFieldDefault(*args{'WMAP','MLS',...},
                   **kwargs{output=True,False[default]})
  ```

4.2 Related magnetic field quantities and conversion

- **name:** __getAlphaGamma

  effect: Computes the B vector inclinations and the polarization position angles assumed to be perpendicular to the projected B field vectors from the field vectors in heliocentric reference frame

  call:
  ```
  __getAlphaGamma(BVectorField_sun)
  ```

- **name:** __getAlphaGamma_fromGal

  effect: Same as __getAlphaGamma() but from field vectors in Galactocentric reference frame.

  call:
  ```
  __getAlphaGamma_fromGal(BVectorField_gal,dotproducts)
  ```

- **name:** __get_Btransverse2_fromGal

  effect: Computes the square of the norm of the projection of the B field vectors on to the plane perpendicular to the line of sight from the field vectors in heliocentric reference frame.

  call:
  ```
  __get_Btransverse2_fromGal(BVectorField_gal,
                             dotproducts)
  ```

- **name:** __getAlphaGammaBtrans2

  effect: computes the B vector inclinations, the polarization position angles (assumed to be perpendicular to the projected B field vectors) and the squared norm of the vector projected in the plane perpendicular to the l.o.s. from the field vectors in heliocentric reference frame.

  call:
  ```
  __getAlphaGammaBtrans2(BVectorField_sun)
  ```

- **name:** __getAlphaGammaBtrans2_fromGal

  effect: Same as __getAlphaGammaBtrans2() but from field vectors in Galactocentric reference frame.

  call:
  ```
  __getAlphaGammaBtrans2_fromGal(BVectorField_gal,dotproducts)
  ```

- **name:** __gal2sun_vector

  effect: Converts vectors from Galactocentric reference frame to heliocentric one

  call:
  ```
  __gal2sun_vector(vector_field,dotproducts)
  ```

- **name:** __get_cylindrical_coord

  effect: Converts a set of coordinates on to cylindrical coordinates

call:
```
__get_cylindrical_coord(coordinates,
                        coordinate_format=
                        {'cartesian','spherical'})
```

4.3 Visualization tool

- **name:** plot_galactic_Bfield_xy_slice

  effect: Produces a map of B field norm (3d) and direction (2d) in the (x, y)-plane of the Galaxy at $z = 0$.

  call:
```
plot_galactic_Bfield_xy_slice(bfield_model,
                              *args{radial_step,xy_limites},
                              **kwargs{x_sun,XYZ_sun,crange})
```

- **name:** plot_galactic_Bfield_xz_slice

  effect: Produces a map of B field norm (3d) and direction (2d) in the (x, z)-plane of the Galaxy at $y = 0$.

  call:
```
plot_galactic_Bfield_xz_slice(bfield_model,
                              *args{radial_step,x_limites,
                                    z_limites},
                              **kwargs{x_sun,XYZ_sun,crange})
```

- **name:** plot_sky_projection

  effect: Produces a sky map of the integrated B field norm (3d)

  call:
```
plot_sky_projection(bfield_model,
                    *args{NSIDE,step_r,limite},
                    **kwargs{x_sun,XYZ_sun,crange})
```

References

Cordes J. M., Lazio T. J. W., 2002, ArXiv Astrophysics e-prints

Fauvet L., Macías-Pérez J. F., Aumont J., Désert F. X., Jaffe T. R., Banday A. J., Tristram M., Waelkens A. H., Santos D., 2011, A&A, 526, A145

Górski K. M., Hivon E., Banday A. J., Wandelt B. D., Hansen F. K., Reinecke M., Bartelmann M., 2005, ApJ, 622, 759

Han J. L., Manchester R. N., Lyne A. G., Qiao G. J., van Straten W., 2006, ApJ, 642, 868

Han J. L., Qiao G. J., 1994, A&A, 288, 759

Jaffe T. R., Ferrière K. M., Banday A. J., Strong A. W., Orlando E., Macías-Pérez J. F., Fauvet L., Combet C., Falgarone E., 2013, MNRAS, 431, 683

Jaffe T. R., Leahy J. P., Banday A. J., Leach S. M., Lowe S. R., Wilkinson A., 2010, MNRAS, 401, 1013

Jansson R., Farrar G. R., 2012a, ApJ, 757, 14

Jansson R., Farrar G. R., 2012b, ApJ, 761, L11

Lee H. M., Draine B. T., 1985, ApJ, 290, 211

Page L., Hinshaw G., Komatsu E., Nolta M. R., Spergel D. N., Bennett C. L., Barnes C., Bean R., et al. 2007, ApJS, 170, 335

Planck Collaboration Int. XIX 2015, A&A, 576, A104

Planck Collaboration Int. XLII 2016, A&A, 596, A103

Planck Collaboration Int. XX 2015, A&A, 576, A105

Planck Collaboration Int. XXII 2015, A&A, 576, A107

Planck Collaboration Int. XXX 2014, ArXiv e-prints

Poezd A., Shukurov A., Sokoloff D., 1993, MNRAS, 264, 285

Ruiz-Granados B., Rubiño-Martín J. A., Battaner E., 2010, A&A, 522, A73

Rybicki G. B., Lightman A. P., 1979, Radiative processes in astrophysics

Sun X.-H., Reich W., 2010, Research in Astronomy and Astrophysics, 10, 1287

Sun X. H., Reich W., Waelkens A., Enßlin T. A., 2008, A&A, 477, 573

Vallee J. P., 1991, ApJ, 366, 450

Waelkens A., Jaffe T., Reinecke M., Kitaura F. S., Enßlin T. A., 2009, A&A, 495, 697